Nocturnal and Seasonal Variations of the Sodium Layer Observed in Northern Japan

Tôhoku Geophys. Journ. (Sci. Rep. Tôhoku Univ., Ser. 5), Vol. 29, No. 4, pp. 151 - 171, 1984

Nocturnal and Seasonal Variations of the Sodium Layer Observed in Northern Japan

FUMIHIKO TOMITA and HIROSHI KAMIYAMA

Upper Atmosphere and Space Research Laboratory,
Tôhoku University, Sendai 980

(Received March 11, 1983)

Abstract: Since the middle of 1980, the vertical profile of the atmospheric sodium layer has been observed by a laser radar at Mt. Zao Observatory (38.1°N, 140.6°E) in northern Japan. The vertical column content of sodium shows a remarkable seasonal variation, being minimum in May and becoming almost twice of the minimum value from October through next February. The height distribution of the sodium density also shows a characteristic seasonal variation. The height at which the density is enhanced predominantly decreases gradually from July to November and then turns up again in the upper region of the layer in next February. The averaged nocturnal variation in the column content shows a post-midnight enhancement maximizing at $1^h \sim 2^h$ L.T. The vertical profile of the density also shows a pronounced nocturnal variation characterized by a wave-like structure. The short period fluctuations (time scale of about 1~2 hr) are superposed frequently on an ordinary nocturnal variation. The density profile in these fluctuations are also characterized, in general, by wave-like features.

1. Introduction

Since the discovery of a radiation at 589.2 nm in the nightglow spectrum in the late 1920's, attempts have been made to obtain informations about the vertical distribution and the abundance of free sodium atoms in the upper atmosphere. Since 1950, the atmospheric sodium layer has been studied by means of twilight resonant scattering techniques and rocket-born photometers, and a comprehensive review paper was given by Hunten (1967). At the end of the 1960's, the tunable laser radar (lidar) technique was developed, and the direct observation of the sodium layer became possible. This lidar technique improved the accuracy of measurements to a large extent and made an epoch-making progress in the study of the sodium layer. Up to now, this technique has been employed by a number of research groups in the world, and series of the observational results have been reported using data obtained at four locations; Winkfield, U.K. (51°N) (Gibson and Sandford, 1972), Haute Provence, France (44°N) (Megie *et al.*, 1978), Urbana, U.S.A. (40°N) (Richter *et al.*, 1981), and São José dos Campos, Brazil (23°S) (Clemsha *et al.*, 1982).

The winter maximum and the summer minimum in the abundance of sodium was already reported based on twilight obsevations as summarized by Hunten (1967). Recent lidar observations by Gibson and Sandford (1971), Megie and Blamont (1977), and Simonich *et al.* (1979) have confirmed the result mentioned above. There are, however, systematic differences among the results reported from different locations, and the latitudinal characteristics were pointed out by Simonich *et al.* (1979). As for the

nocturnal variation, the lidar technique has given an important information about the vertical profile of the sodium layer. One of the most characteristic features is the wave-like structure showing a downward progression of the phase throughout the night, and is suggested to be associated with the propagation of gravity waves (Blamont *et al.*, 1972; Shelton *et al.*, 1980) or tides (Kirchhoff and Clemsha, 1973; Clemsha *et al.*, 1982). In early days in the history of the lidar technique, observations were possible only in the nighttime because of a much higher noise level in daytime. But recently, excellent developments in the lidar system have been made and the measurement of the daytime sodium layer becomes possible (Gibson and Sandford, 1972; Clemsha *et al.*, 1982). Especially, Clemsha *et al.* (1982) have succeeded in obtaining the diurnal variation of the sodium layer by making continuous observation over a number of complete diurnal cycles, and showed the existence of pronounced semidiurnal oscillations in the vertical column abundance and the height distribution of sodium. They also pointed out that the semidiurnal oscillation is dominant in the higher region of the layer, whereas in the lower extreme of the layer a diurnal oscillation predominates.

In 1972, the lidar observation of the sodium layer was also successful at Mt. Zao Observatory (38°N) located in northern Japan (Aruga *et al.*, 1974), but the height resolution was not satisfactory because of an insufficient output energy of the transmitter. In 1980, a new system which consists of a transmitter having a much higher output power in the sufficiently narrow bandwidth and an improved receiving system was developed, and a more accurate observation has since been available at our observatory. The instrumentation of this system were already described, in detail, in the previous paper (Kamiyama *et al.*, 1981). The purpose of the present paper is to present the characteristics of the sodium layer relating to its seasonal, nocturnal, and short period variations based on the data taken during 73 nights in the period from August, 1980 to December, 1982, at Mt. Zao (38°N).

2. Outline of the Lidar System and Data Analysis

Principal characteristics of the lidar system used now at Mt. Zao Observatory are given in Table 1. The solution of 1×10^{-4} mol/l of rhodamine 6G dissolved in isopropanol is utilized as the source material for laser emission. The spectral narrowing and tuning to the sodium D_2 line are performed by employing a set of two tilted Fabry-Perot filters inside the cavity and the third Fabry-Perot filter acting as the output mirror as

Table. 1 Characteristics of the lidar system

Transmitter		Receiver	
Wavelength	589.0 nm	Effective area	0.2 m^2
Divergence	3 mrad	Field of view	5 mrad
Transmitted bandwidth	16 pm	Bandwidth	2 nm
Repetition rate	0.25 Hz	Height resolution	1.5 km
Output energy	80 mJ/pulse		
Pulse duration	2.2 μs FWHM		

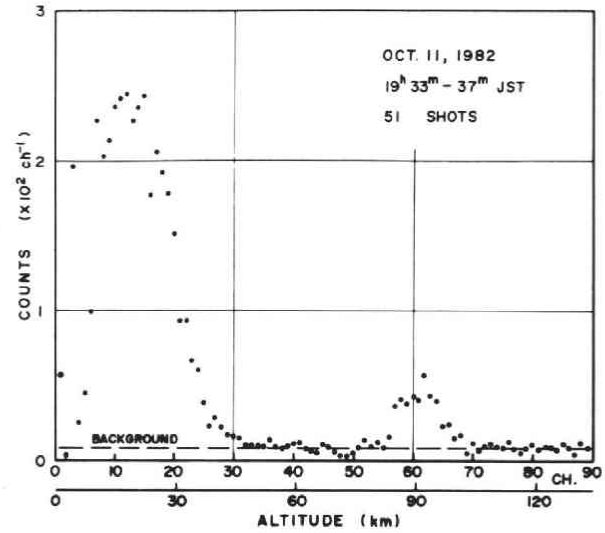

(a)

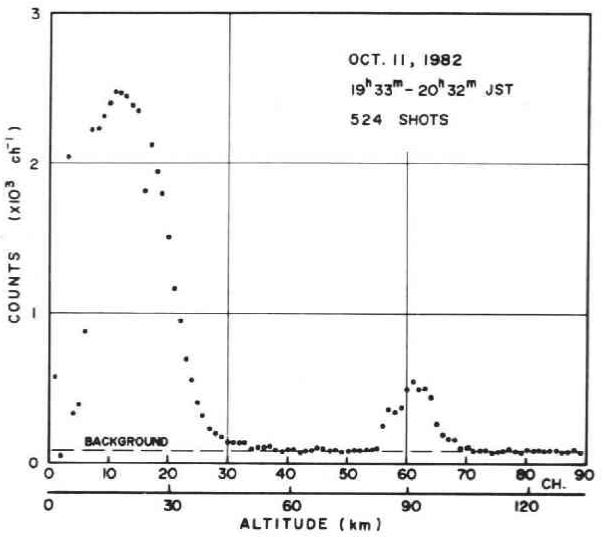

(b)

Fig. 1 Realtime data of return signal counts. The background noise level decided from the counts in the channels from 151 to 250 is also indicated. (a) Return signal counts integrated for 4 minutes, $19^h33^m \sim 37^m$ JST on Oct. 11, 1982, during which 51 laser pulses were transmitted. (b) Same as in (a), but integrated for 59 minutes, $19^h33^m \sim 20^h32^m$ JST on the same day, during which 524 laser pulses were transmitted.

well. The output wavelength is continuously monitored by using a sodium resonance cell, a spectrometer, and a Fabry-Perot interferometer provided with the reference spectrum of a sodium lamp. The duration of the photon counting for each channel in the receiving system is set at 10 μsec corresponding to the range resolution of 1.5 km. The

counts of return signals for each channel are accumulated in MCA (multichannel analyzer) for four minutes while about 60 shots of laser pulses are ordinarily transmitted. The accumulated counts stored in MCA are transferred to a floppy disk, being written in a given format, with the aid of the micro computer system within one minute before the next four mintutes period of the measurement starts. Examples of the height profiles of the return signals are given in Figs. 1a, b for the height range up to 130 km. The depression of counts for the region below 25 km is concerned with the limit of the pulse pair resolution of our counting system and the geometry of the receiving telescope with respect to the transmitting telescope (Kamiyama *et al.*, 1981).

The calibration of the absolute sodium density has been carried out by adopting the method established by previous works (*e.g.*, Aruga, 1972; Megie and Blamont, 1977; Simonich *et al.*, 1979). Assuming that almost all of the atmospheric attenuation affecting the laser beam takes place in the troposphere and the lower stratosphere, the sodium density, N_{Na}, at a given altitude, h_{Na}, is given by

$$N_{Na}=N_R\frac{n_{sNa}(d\sigma/d\Omega)_R\ h_{Na}^2}{n_{sR}(d\sigma/d\Omega)_{Na}\ h_R^2}\ , \tag{1}$$

where N_R denotes the number density of the Rayleigh scattering molecules at a reference altitude, h_R, n_{sNa} and n_{sR} the received counts of the signals from altitudes, h_{Na} and h_R, due to the resonant and the Rayleigh scatterings, respectively. Here, $(d\sigma/d\Omega)_{Na}$ and $(d\sigma/d\Omega)_R$ are the differential back scattering cross sections for the resonant and the Rayleigh scatterings, denoting the scattering angle by Ω, respectively. When C is defined as

$$C=\frac{N_R}{n_{sR}\ h_R^2}\ , \tag{2}$$

one may obtain from the usual laser radar equation

$$C=\{\ n_o\ (d\sigma/d\Omega)_R\ \Delta h\ K\ A\ T_R^2\ \}^{-1}. \tag{3}$$

Here, n_o denotes the number of the transmitted photons, Δh the height range concerned, K the overall efficiency of the lidar system, A the effective area of the receiving telescope, and T_R the atmospheric transmittance. Thus, the value, C, might be expected simply to be constant throughout the region above a certain height, say 15 km, above which the atmospheric attenuation can be neglected. Practically, however, C-value varies with height in some altitude ranges. One of the reasons for this change in C is that the counting rate, n_{sR}, for the lower atmospheric region (<25 km) is suppressed to some extent due to the limit of the pulse pair resolution of our photon counting system. Another reason is concerned with the Mie scattering which is not taken into account in (1). On the other hand, C may vary with time because the number of the transmitted photons, n_o, the atmospheric transmittance, T_R, and the overall efficiency of the lidar system, K, can be changed. The temporal change in C, however, does not affect the estimation of the sodium density, N_{Na}, because the counting rates due to the resonant and the Rayleigh scatterings, n_{sNa} and n_{sR}, respectively, are affected in the same proportion to the changes in n_o, T_R, and K.

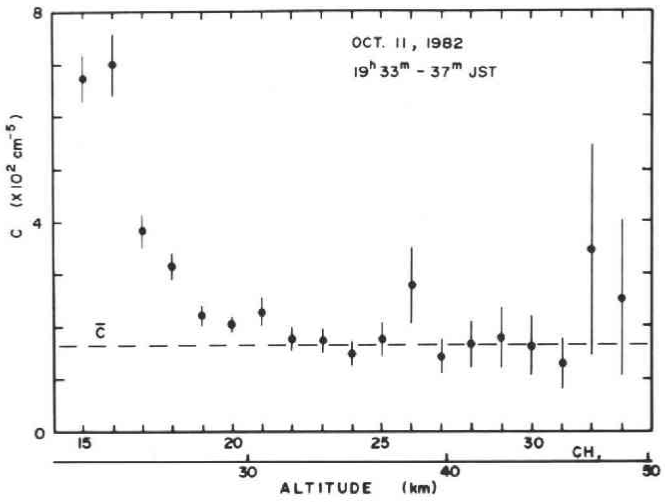

(a)

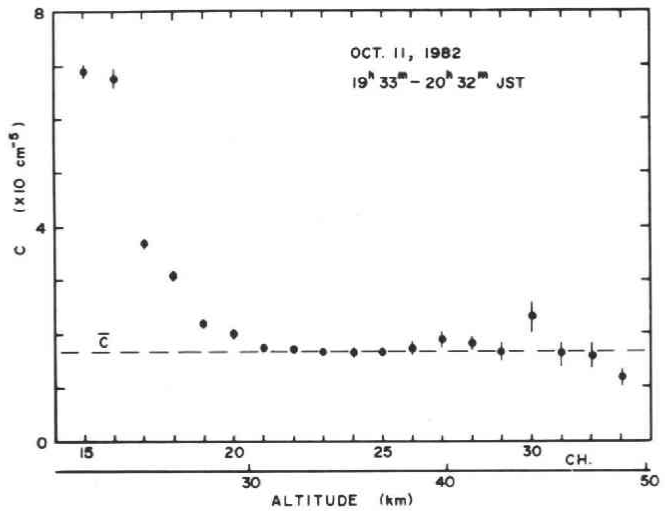

(b)

Fig. 2 The C-values plotted as a function of the channel and height. Error bars correspond to the statistical errors due to the limited count rates of return signals. The adopted $\bar{C}$-value which is determined by averaging C-values in the selected channels is shown by the dashed straight line. (a) 19h33m~37m JST, on Oct. 11, 1982. (b) 19h33m~20h32m JST, on the same day.

Then, the value, C, is calculated from (2) as a function of height by using observed data for n_{sR} and the assumed model for N_R. The vertical distribution of the atmospheric density is calculated by employing the temperature data obtained at Sendai District Meteorological Observatory for the region below 30 km and those given in the U.S. Standard Atmosphere Supplements (1966) for the upper region. Examples are given in Figs. 2a, b, which show C-values as the function of the channel number of MCA

or altitude. Fig. 2a is calculated from data for n_{sR} taken in the period from 19^{h}33^m to 19^{h}37^m JST on Oct. 11, 1982. Adopting the values for channels from 22 through 30, except for 26, the averaged C-value is determined as $\bar{C}$. In Fig.2b, C-values are calculated based on the data taken in the period from 19^{h}33^m to 20^{h}32^m JST on the same day. The constancy of C with respect to height is considerably improved, and $\bar{C}$ is determined by averaging the values for channels from 21 through 32, except for 27, 28, and 30. In case where $\bar{C}$ can not be determined uniquely because of a steps-like change in C, a probable range of $\bar{C}$ is estimated and the corresponding uncertainty in the sodium density is taken into account as an experimental error. As for the differential back scattering cross sections, $(d\sigma/d\Omega)_R$ is quoted from the literature (Handbook of Geophys. and Space Environments, 1965), and $(d\sigma/d\Omega)_{Na}$ is obtained according to Simonich *et al.* (1979).

The laser bandwidth was measured with a Fabry-Perot interferometer of 60 pm free spectral range and a microdensitometer, and was found to be 16 ± 1 pm. Then, the uncertainty in the evaluation of $(d\sigma/d\Omega)_{Na}$ is approximately $\pm6\%$. Owing to the strict temperature control to 0.005°C for the filters, the tuning is sufficiently stable throughout a night. Another uncertainty in the determination of the absolute sodium density is introduced statistically due to the limited photon count, it is estimated to be approximately $\pm14\%$ for a four minutes integration time, and $\pm4\%$ for one hour integration time. The error arising from an uncertainty in the vertical distribution of the atmospheric density is considered to be much smaller. The results of the observation will be prestented in following sections.

3. Seasonal Variation

Column contents of the atmospheric sodium are calculated for each vertical profile

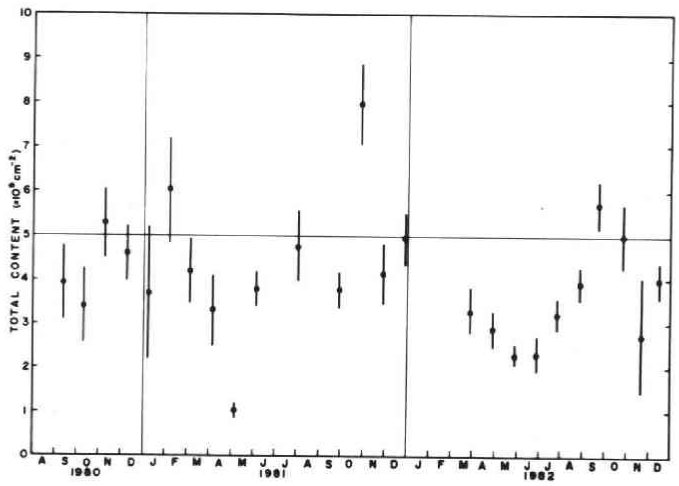

Fig. 3 Seasonal variation of the nighttime column content of sodium. The error bars represent either the probable error of the statistics or the uncertainty of the calibration, whichever is larger.

of the sodium density derived from hourly integrated data, and are averaged over each observational period which is scheduled for about two weeks centered around every new moon epoch. These averaged values for the period from September, 1980 to December, 1982 are plotted in Fig. 3. Error bars represent either the probable error of the dispersion or the extent of uncertainty in our estimation whichever is larger. Because of an unfavorable weather condition, the number of observations in winter is limited. In order to estimate a value at the middle of each month, linear interpolations between adjacent points in Fig. 3 are adopted. Then, taking averages for respective months, the seasonal variation in the monthly abundances is plotted in Fig. 4. One may see the maximum of

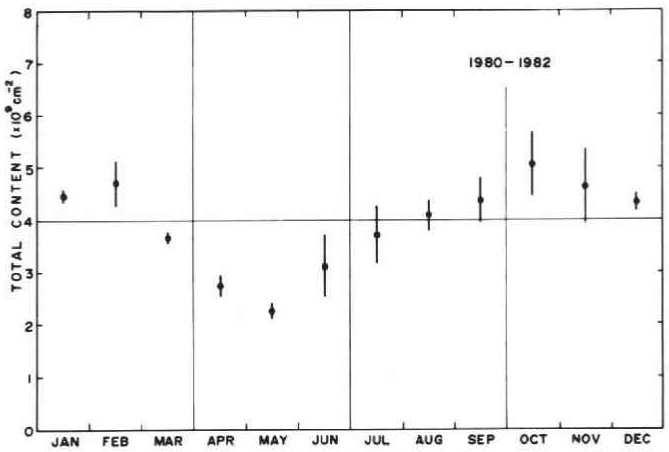

Fig. 4 Averaged seasonal variation of the nighttime column content of sodium. The error bars represent the probable error.

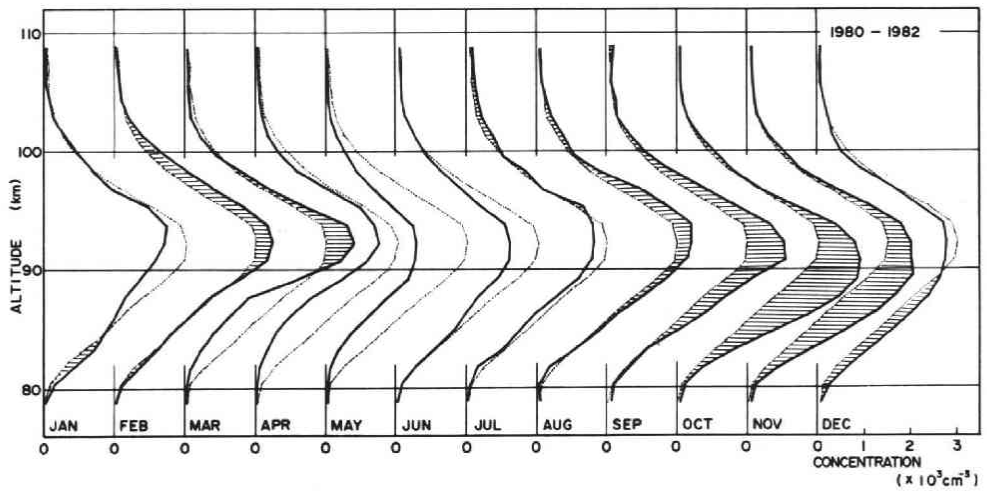

Fig. 5 Averaged seasonal variation of the vertical distributions of sodium density (solid lines) and the annually averaged profile (dotted lines). The enhanced regions are indicated by hatching.

5.1×10^9 atoms cm^{-2} in October, followed by a slight depression in December, the secondary maximum of 4.7×10^9 atoms cm^{-2} in next February, and the minimum of 2.3×10^9 atoms cm^{-2} in May. Such a seasonal variation showing the maximum in winter and the minimum in early summer is consistent with the results so far reported (Gibson and Sandford, 1971; Megie and Blamont, 1977; Simonich *et al.*, 1979). Our result obtained at Mt. Zao (38°N) characterized by the broad maximum in winter seems to be, however, of a plateau type which is not similar to those obtained at higher latitudes (44°N, 51°N), but common to that at a lower latitude (23°S).

To inquire further into the seasonal variation, the monthly profiles of the density distribution are shown in Fig. 5. In this figure, sodium density profiles averaged over each month are given by the solid lines, together with the annually averaged profile shown by the light dotted lines for reference. The regions where the density enhances over the annually averaged profile are indicated by hatching. One may see a characteristic seasonal variation in the structure of the layer. The altitude of the hatched region decreases gradually from July to November and then turns up again in the upper part of the layer in next February. The peak altitude shows obviously the seasonal variation with the amplitude of about 4.5 km. This type of variation of the peak altitude is similar to the results obtained at higher latitudes (44°N, 51°N), whereas no variation has been shown at a lower latitude (23°S). The seasonal characteristics of the structure of the layer can be illustrated in a different manner as shown in Fig. 6. This contour map gives the difference between the height distribution of the sodium density (cm^{-3}) and that of the annual average as the function of month, and the regions where the absolute difference exceeds 200 cm^{-3} are indicated by the two different shading areas corresponding to their signs. The peak altitude averaged over a year is also indicated in the figure. It is evident that the amplitude of the seasonal variation is much larger in the bottom side of the layer than in the higher part. The sodium density shows the minimum in April and the maximum in November in the lower part of the layer, whereas in the higher part the density shows minimum in May, the maximum in September, being followed by the secondary maximum in February.

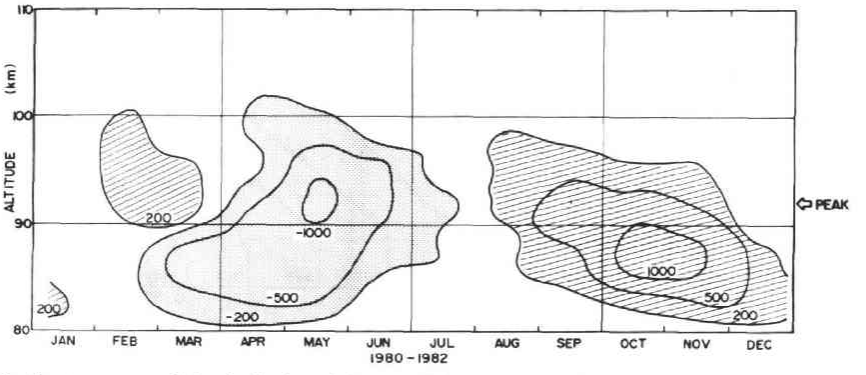

Fig. 6 Contour map of the deviation of the monthly average profiles from the annually averaged profile. Deviation of the density is given in cm^{-3}.

4. Nocturnal Variation

Various sorts of nocturnal variations in the sodium layer have so far been reported. One of the most interesting features is the wave-like structure showing a downward progression of the phase angle (*e.g.*, Rowlett, *et al.*, 1978; Simonich *et al.*, 1979; Clemsha *et al.*, 1982).

The averaged nocturnal variations of the column content of sodium observed at Mt. Zao are shown in Figs. 7a, b, c, which show the three sorts of trends depending on the range of the nocturnal variation, respectively. In order to obtain the nocturnal trend from 20^h to 4^h JST, only the data taken continuously for more than five hours are selected for statistics. In order to avoid an influence of a peculiar variation obtained in a certain night when the level of the observed values is relatively high and consequently a range of the variation can be large, the following procedure is employed. The averaged level of sodium contents for each night is normalized to the averaged level of whole data, and the relative variation in each night is reduced or enhanced by a factor corresponding. In Fig. 7a for the small range of the variation (range$<2\times10^9$ atoms cm^{-2}), although the result at 4^h JST is not presented because of the insufficient number of data, a general tendency is seen that the column content increases toward dawn. In the cases of greater amplitudes of the variation, one may see the post midnight enhancement maximizing at about 1^h JST. This characteristic is similar to the result reported by Clemsha *et al.* (1982), whereas Simonich *et al.* (1979) found no obvious variation in their statistical result.

Some examples showing characteristic variations in the vertical profile of the sodium density are given in Figs. 8 through 11. Each of the profiles is obtained from hourly integrated data and is shown by the solid line. The averaged profiles for the respective nights are also shown for reference by the dotted lines in the same way as in Fig. 5. Also shown in the upper panel is the trend of the hourly values of the column content. It is pointed out that the pronounced feature common in these examples is the decrease, with time, in the altitude where the density makes enhancement. In one of the most remarkable variation in Fig. 8 (Mar. 11~12, 1981), the height of the density enhancement descends at the rate of about 2 km hr^{-1} on an average accompanying the increase in the column content. In this figure, one may see the much more pronounced nocturnal variation in the sodium density in the lower part of the layer than in the higher part and also the downward phase progression. These characteristics are shown more obviously by contour maps in Figs. 12a, b. In Fig. 12a, the differences between each profile and the averaged profile over a night are shown in terms of the sodium density (cm^{-3}), while in Fig. 12b they are given in the percentage deviation from the average at respective height. The areas for large deviations of contents from the average in the both figures are indicated separately by shading in the same way as in Fig. 6. One can clearly see the enhanced variation of the sodium density in the lower part of the layer in Fig. 12a, and the downward phase progression in Fig. 12b. In the latter figure, the wave-like structure reveals a vertical wavelenght of 14~20 km and a period of about 12 hr.

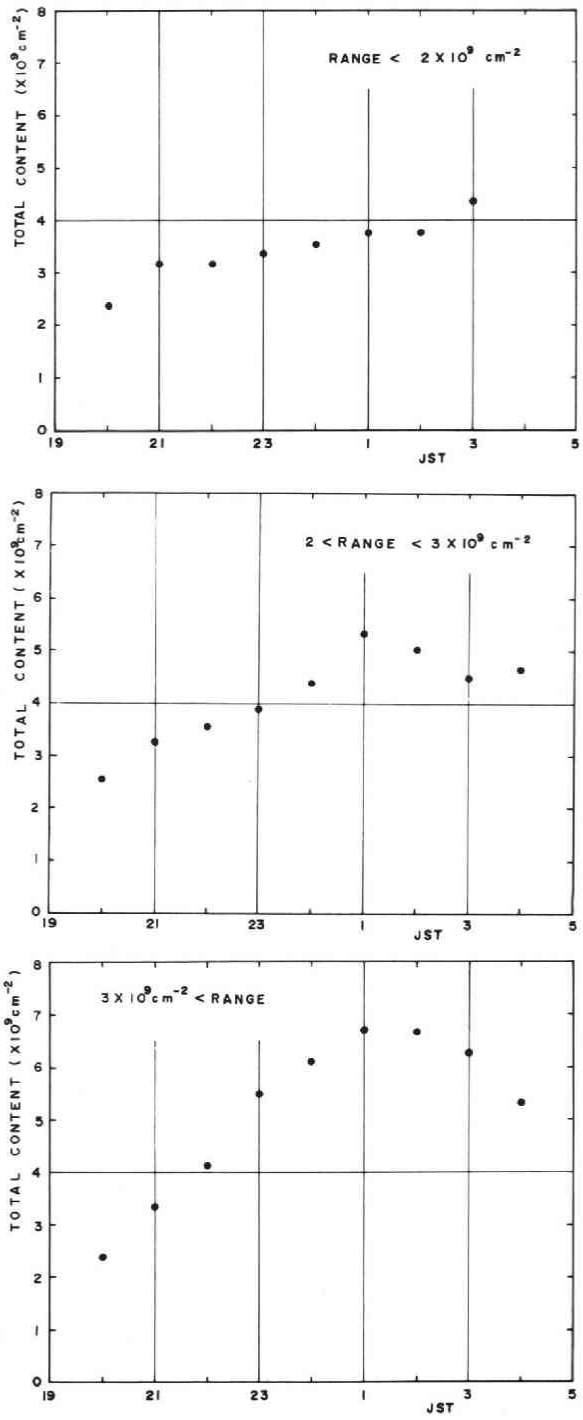

Fig. 7 Averaged nocturnal variations in the column content of sodium derived from data classified according to the range of the variation: (a) for nights in which the range is less than 2×10^9 cm^{-2}. (b) for nights when 2×10^9 cm^{-2} <range<3×10^9 cm^{-2}. (c) for nights when 3×10^9 cm^{-2} <range.

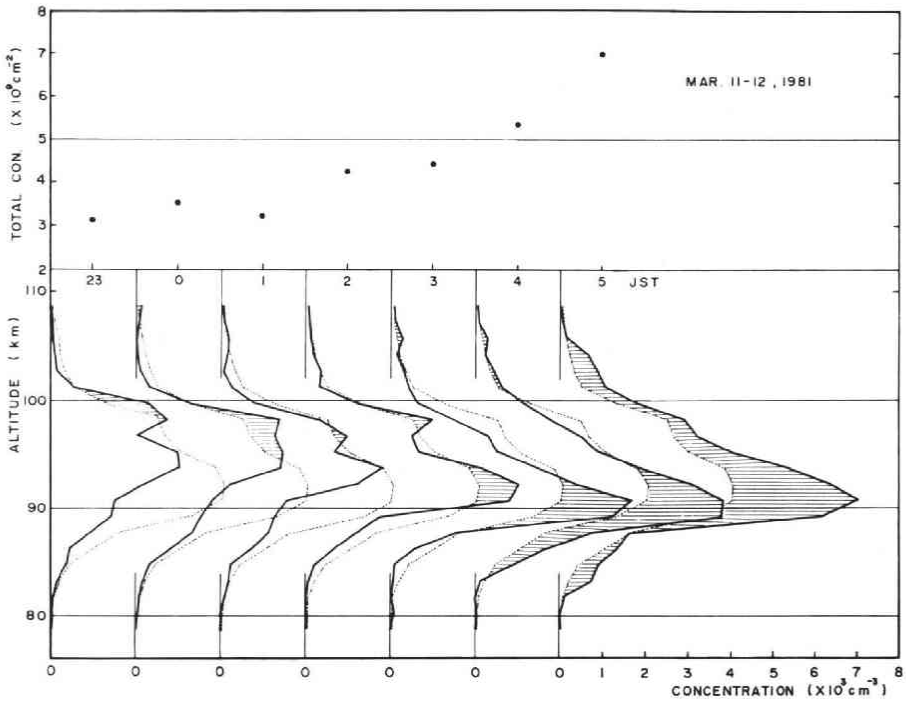

Fig. 8 An example of the nocturnal variation of the density profile derived from hourly integrated data (solid lines), the nocturnally averaged profile (dotted lines), observed on Mar. 11 ~12,1981. The enhanced regions are indicated by hatching. The column contents are also plotted in the upper panel.

This wave motion seems to be of the same type as semidiurnal oscillations reported by Clemsha *et al.* (1982). Another example given in Fig. 9 (Apr. 7~8, 1981) shows such a feature more clearly as illustrated in Figs. 13a, b. In Fig. 13b, the vertical wavelength is estimated to be 16~22 km, and the striped pattern of the percentage density deviation is much more obvious than in Fig. 12b. In the case of an example given in Fig. 10 (Jul. 13 ~14, 1982), a narrow peak at the altitude of about 97 km appeared suddenly at about 23^h JST and its altitude decreases slowly at a rate of 0.4~0.5 km hr^{-1}. Fig. 11 (Oct. 21~22, 1982) is an example showing the existence of semidiurnal oscillations in the column content and the vertical distribution. The oscillations in the sodium density at the altitude of 82 km and 93 km, respectively, were of completely out-of-phase indicating the vertical wavelength of 22 km and period of about 12 hr.

Our data collections have been carried out usually at every five minutes as mentioned earlier. Therefore, the variation of the vertical profile of the sodium layer can be studied with a higher time resolution. In Fig. 8 (Mar. 11~12, 1981), the secondary peak at an altitude of 97~98 km could not be observable at about 3^h JST, and at the same time the main peak at a lower altitude showed remarkable enhancement. This event was illustrated in Fig. 14 at 20 minutes intervals by profiles estimated from ten minutes integrated data. The averaged profile for the period from 0^h00^m to 3^h10^m is also shown

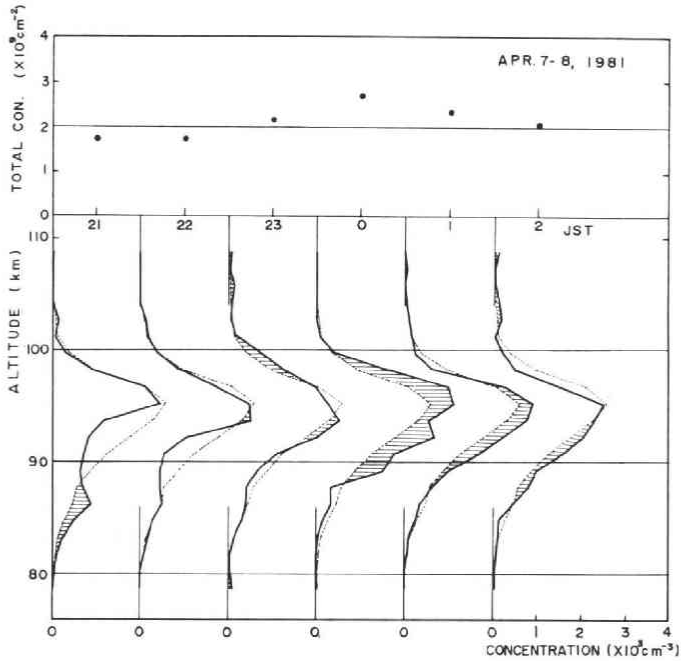

Fig. 9 Same as in Fig. 8, but for the results on Apr. 7~8, 1981.

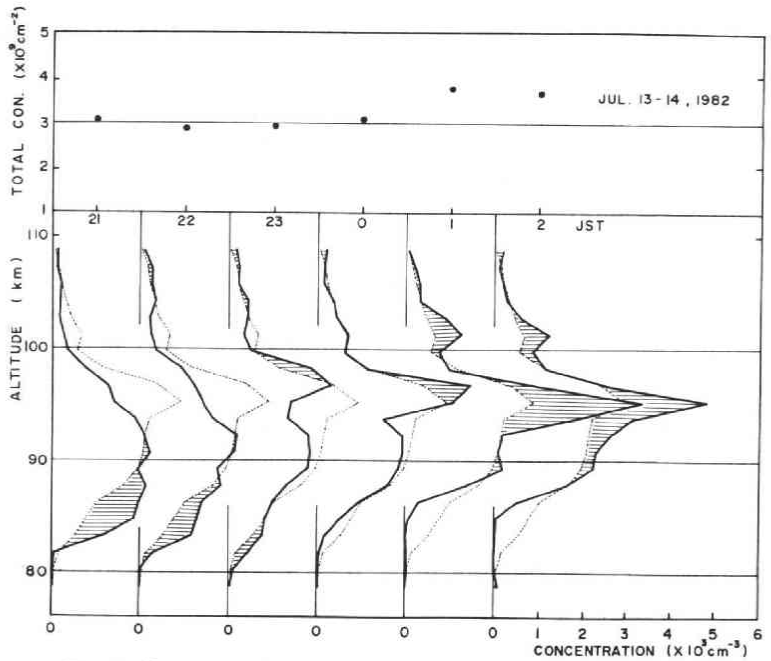

Fig. 10 Same as in Fig. 8, but for the results on Jul. 13~14, 1982.

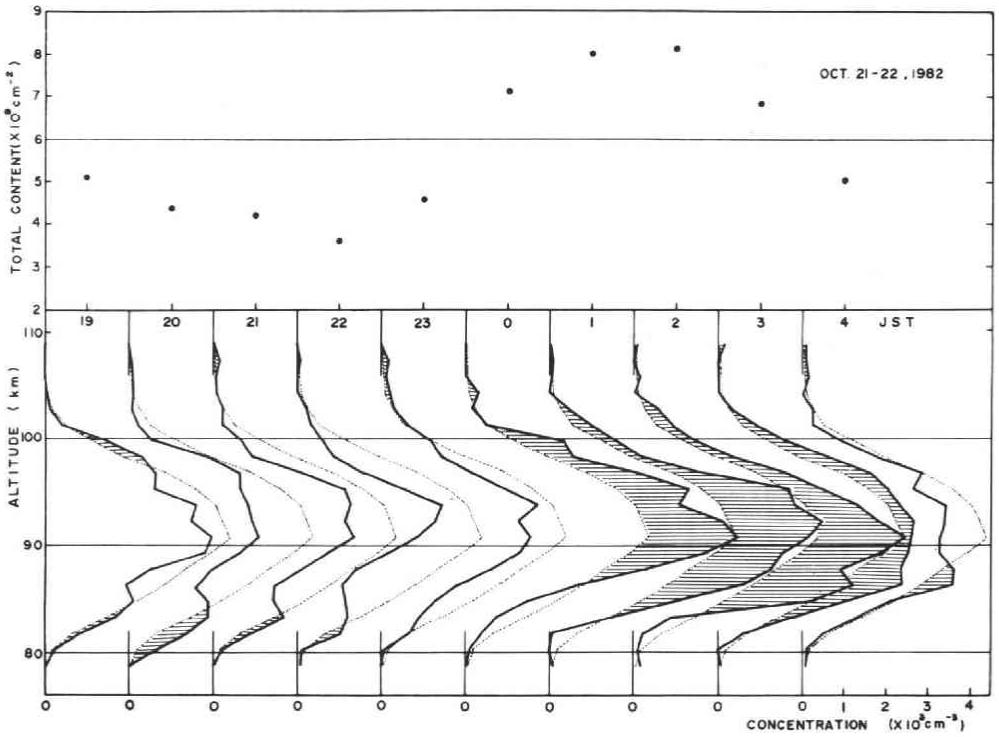

Fig. 11 Same as in Fig. 8, but for the results on Oct. 21~22, 1982.

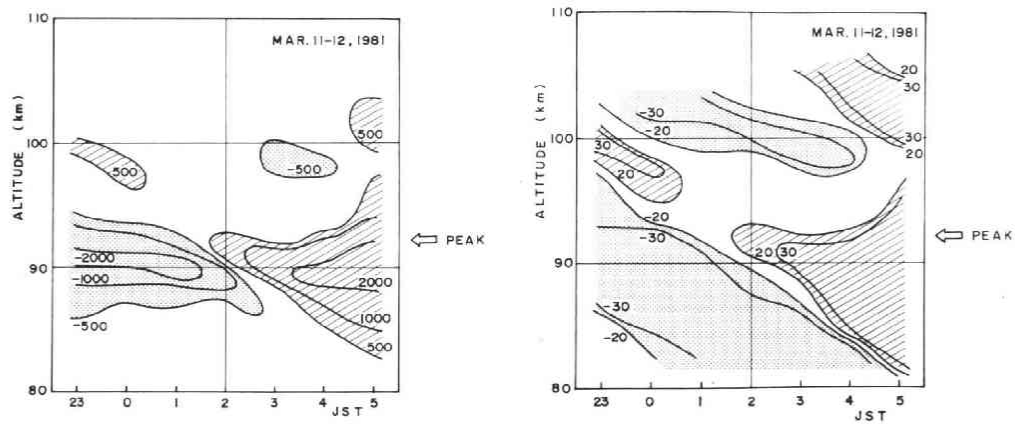

Fig. 12 Contour map of the difference between the hourly profiles and the nocturnally averaged profile observed on Mar. 11~12, 1981. (a) The density contour is given in cm^{-3}. (b) The percentage deviations from the nocturnal average.

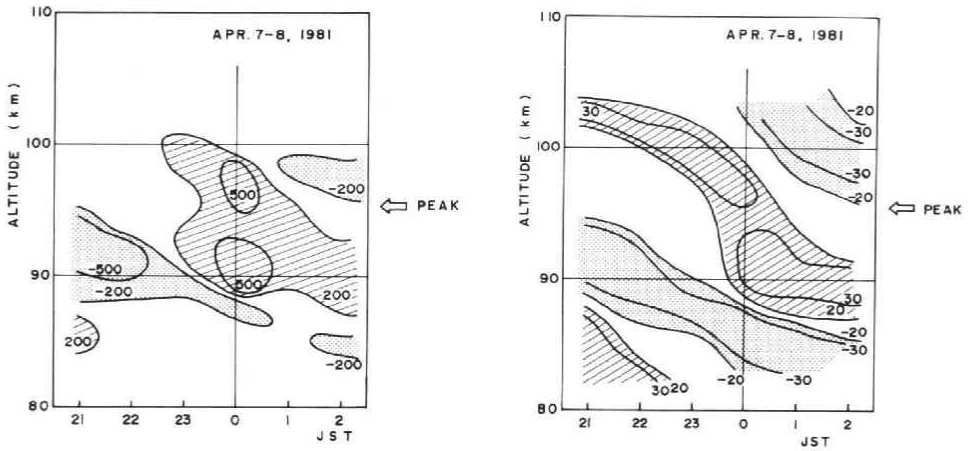

Fig. 13 Same as in Fig. 12, but for the results on Apr. 7~8, 1981.

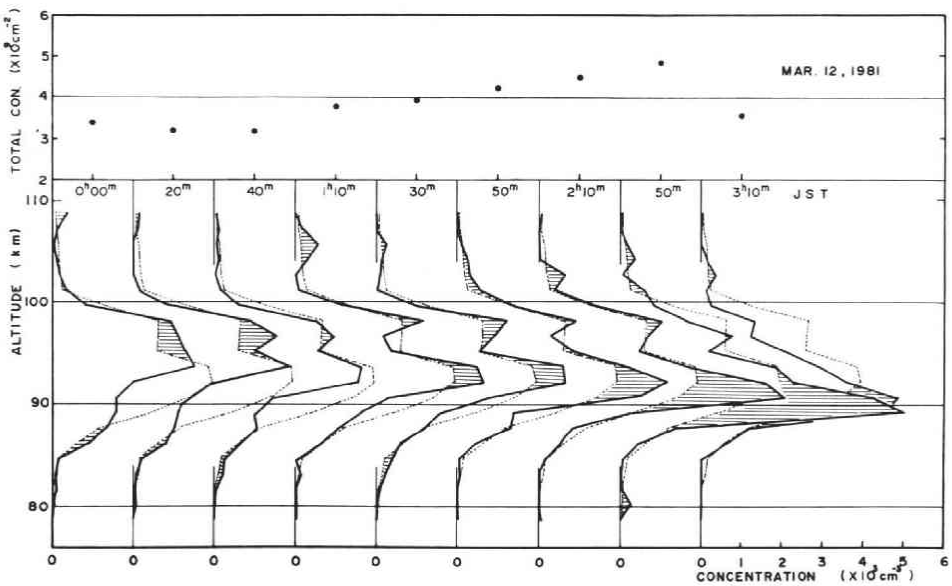

Fig. 14 Profiles (solid lines) derived from ten minutes integrated data, the average profile (dotted lines), and column content (the upper panel) observed during the period, 0^h00^m~3^h10^m JST, on Mar. 12, 1981.

by dotted lines. From the figure, this event can also be understood as the result of a wave motion in the sodium layer. Fig. 15 (Jul. 13~14, 1982) shows the details of the variation in the profile from 22^h35^m to 1^h35^m in the same way as in Fig. 14. In this figure, the narrow peak appeared suddenly at the altitude of about 97~99 km at 22^h55^m JST. The density of the peak decreased toward 23^h35^m JST and then turned to increase toward 1^h15^m JST. It is obvious that the increase of the peak density from 23^h55^m to 1^h15^m was

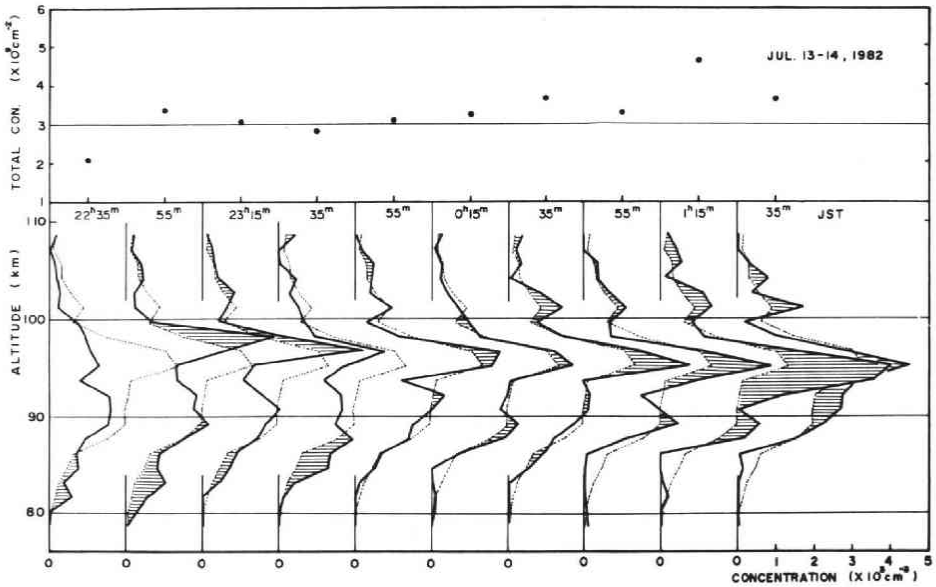

Fig. 15 Same as in Fig. 14, but during the period, $22^h35^m \sim 1^h35^m$ JST, on Jul. 13~14, 1982.

accompanied with a decrease in the altitude of the peak. These features are thought to be reflecting a combined effect of atmospheric oscillations and sodium chemistry.

5. Short Period Fluctuations

As mentioned in the previous section, short period fluctuations in the sodium density profile are suggested to be quite useful for better understanding of the mechanism dominating in the sodium layer. For example, Fig. 16 illustrates the nocturnal variation in the sodium column content during the night, Jul. 31~Aug. 1, 1981. Although column contents are estimated at every five minutes, running averages of adjacent three values are plotted in order to smooth out noisy fluctuations. One may see in this figure that short period variations characterized by a period of about one hour or so are superposed on the general increasing trend. In the shaded portion of this figure, the sodium content shows an enhancement by more than 20% within 20 minutes. The nocturnal variation of the profile based on hourly integrated data for this night is shown in Fig. 17. The descending feature of the wave-like structure can obviously be seen in this figure. The secondary peak which appeared below 90 km during the period from 2^h to 3^h JST is of particular interest. Vertical profiles of the sodium density in this period are shown at five minutes intervals in the lower panel of Fig.18. Each of the profiles is provided by employing 15 minutes integrated data in order to reduce noisy fluctuations arising from the photon-counting statistics. The dotted lines represent the averaged profile for the period concerned, and column contents are shown in the upper panel of the figure. One can see a downward shift of the wave-like structure which is similar to the result shown by Shelton *et al.* (1980). The density variations at the altitude of 83 km and 95 km are

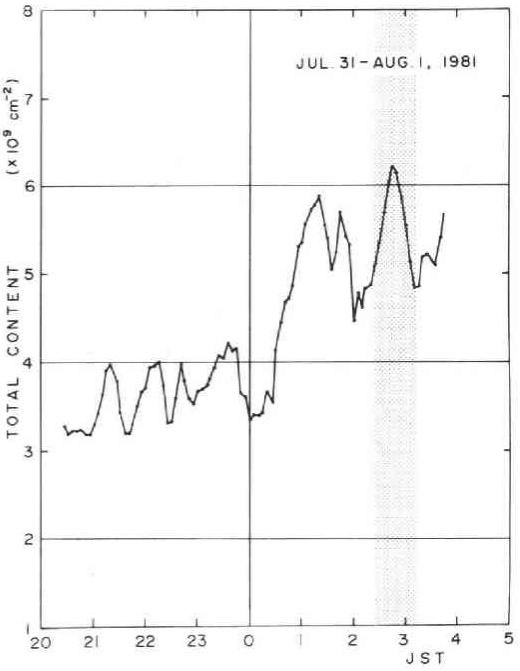

Fig. 16 Nocturnal variation of the sodium column content observed on Jul. 31 ~Aug. 1, 1981. The running averages of 3 adjacent results based on 5 minutes integrated data are plotted in this figure. The period during which details are shown in Fig. 18 is indicated with shading.

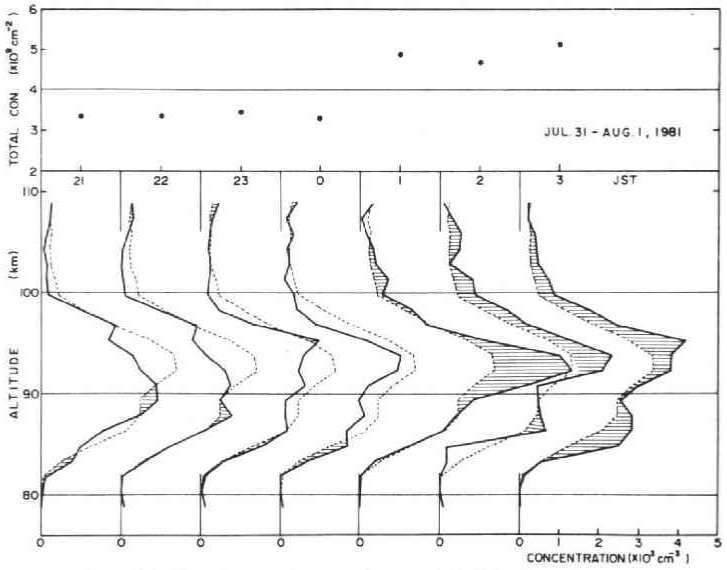

Fig. 17 Hourly density profiles on Jul. 31~Aug. 1, 1981.

in-phase, and those at 89 km and 98 km are also in-phase, whereas both of the pairs are out-of-phase. From these characteristics, it is obvious that there are short period oscillations having a vertical wavelength of 9~12 km and a period of about 60 min. This kind of oscillations were also reported by Rowlett *et al.* (1978). In another example

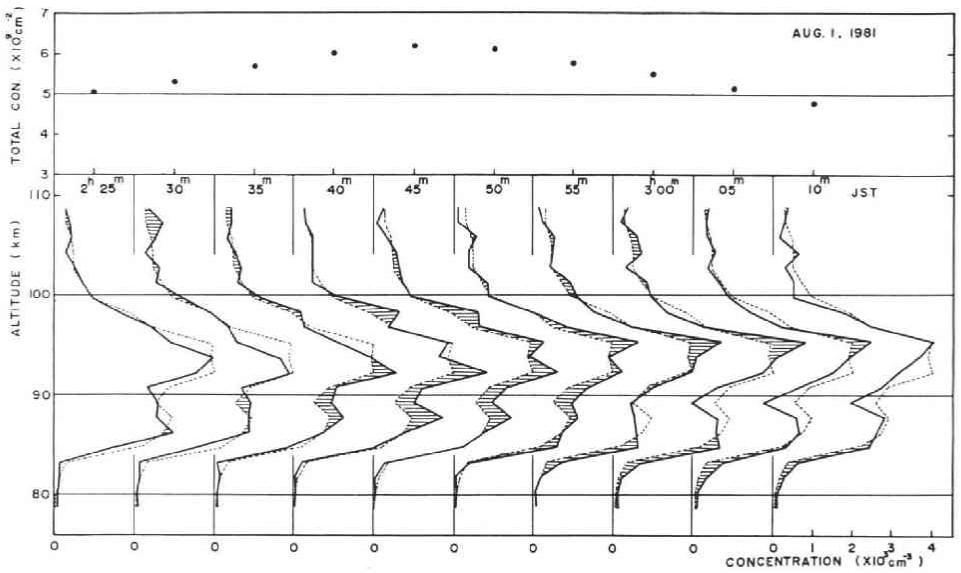

Fig. 18 An example of short period fluctuations of the column content, the profiles (solid lines) at every five minutes, and the averaged profile (dotted line) observed during the period, 2^h25^m $\sim 3^h10^m$ JST, on Aug. 1, 1981.

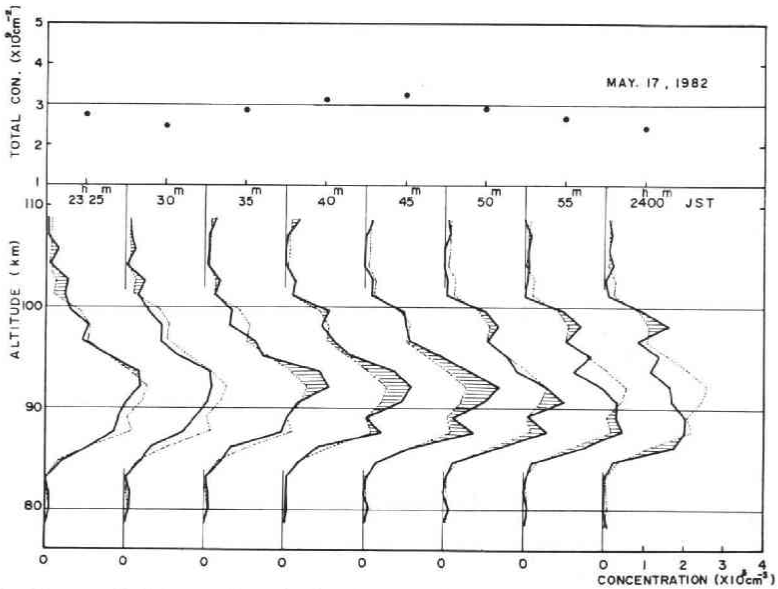

Fig. 19 Short period fluctuations during the period, $23^h25^m \sim 24^h00^m$ JST, on May 17, 1982.

($23^h25^m \sim 24^h00^m$ JST, May. 17, 1982) shown in Fig. 19, the variations of the sodium density at the altitudes of 87 km and 98 km, respectively, seem to be in-phase, whereas the phase of the variation at 92 km is quite different from that of the above pair. In this event, the

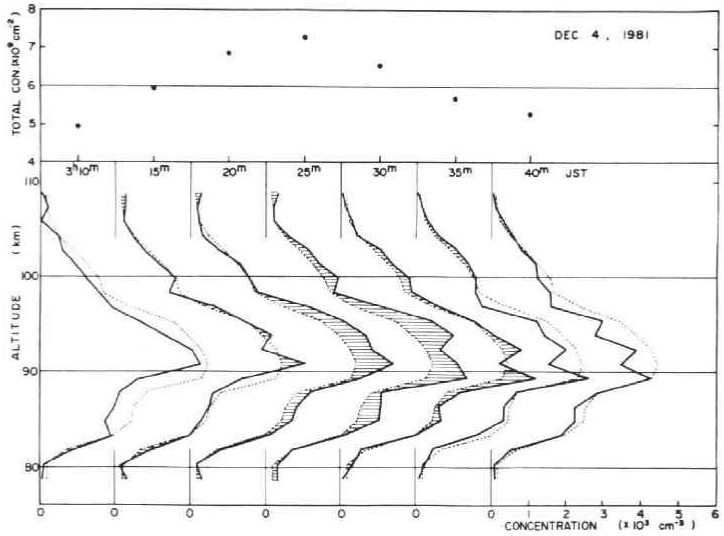

Fig. 20 Short period fluctuations during the period, $3^h10^m \sim 3^h40^m$ JST, on Dec. 4, 1981.

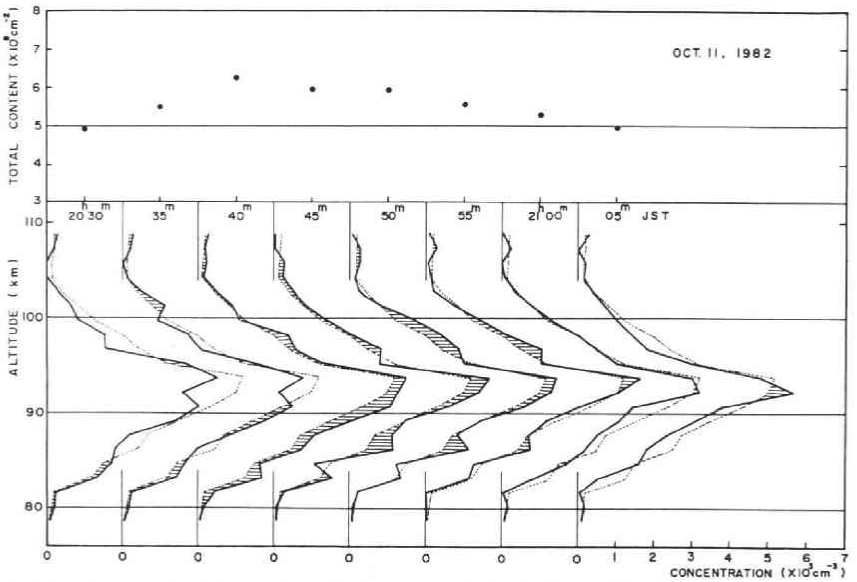

Fig. 21 Short period fluctuations during the period, $20^h30^m \sim 21^h05^m$ JST, on Oct. 11, 1982.

vertical wavelength is found to be about 11 km and the period is estimated to be 30~50 min.

There is another kind of events in which the sodium density is enhanced simultaneously at almost entire height range concerned. In the lower panel of Fig. 20 ($3^h10^m \sim 40^m$ JST, Dec. 4, 1981), one may see that the sodium density increased at almost all altitudes in accord with the enhancement of the column content shown in the upper panel of the figure. Note that, however, the altitude of the maximum density decreased

gradually throughout this period. In another example shown in Fig. 21 ($20^h30^m \sim 21^h05^m$ JST, Oct. 11, 1982), the sodium density enhanced simultaneously at almost all altitudes following the increase of the column content. It is not clear now whether this type of fluctuations in the sodium density at almost all altitudes are caused by a kind of a wave motion in the atmosphere or by the deposit of sodium atoms into the atmosphere at the altitudes concerned.

6. Discussion and Summary

The column content of the nighttime sodium layer show a pronounced seasonal variation in northern Japan (38°N), showing the maximum in October, a slight depression in December, the secondary maximum in next February, and the minimum in May. This variation is of same type as that observed at a low latitude in the southern hemisphere (23°S), with the phase shift of a half year, by Simonich *et al.* (1979) rather than those shown at 44°N by Megie and Blamont (1977) and at 51°N by Gibson and Sandford (1971) in the northern hemisphere. The winter (December-January) to summer (June-July) ratio in the column content at 38°N is found to be 1.3 which lies between those obtained at Kitt Peak (32°N), U.S.A., from the twilight observation (Hunten, 1967) and at Haute Provence (44°N), France, by the lidar observation (Megie and Blamont, 1977), and is consistent with the result reported by Simonich *et al.* (1979). The peak altitude of the layer is low in winter and high in early summer, the range of the seasonal change being about 4.5 km. This value corresponds to an intermediate characteristic between the result at higher latitudes (44°N, 51°N) and that at a lower latitude (23°S) where no seasonal change is reported. The height where the density is enhanced predominantly decreases gradually from July to November and then turns up again in the topside region of the sodium layer in next February. This characteristic seasonal change in the profile of the sodium layer is thought to be closely related to the annual variation of the atmospheric composition involved in sodium chemistry in the altitude region concerned.

The nocturnal sodium layer shows a large variety of variations, reflecting not only a possible change in the source of atmospheric sodium but also a combined effect of the dynamics and chemistry of the sodium layer.

The averaged nocturnal variations of the sodium column content shown in Figs. 7a, b, c are considered to be due to the dynamical effect of the wave motion. From our observed data, results shown in Fig. 8 through Fig. 11 are selected as particularly clear examples. In these results, the profiles of the sodium density are superposed by wave-like structures with a vertical wavelength of 14～22 km and the downward phase progression with speeds ranging from 0.4 to 7 km hr^{-1}. Although the downward phase velocity is consistent with early works (Rowlett *et al.*, 1978; Simonich *et al.*, 1979), the vertical wavelength found from the present observations is larger than that reported in the previous paper but is smaller than that reported by Clemsha *et al.* (1982).

The short period fluctuations having periods of about 1 hr or so are frequently superposed on a nocturnal variation of the sodium layer. Most of them are accompanied by the descending wave-like structures in which the vertical wavelength is esti-

mated to be 9~12 km. Although these features are consistent with the results reported by Rowlett *et al.* (1978) and Shelton *et al.* (1980), a more detailed study will be required to confirm that these perturbations are due to the propagation of gravity waves (Shelton *et al.*, 1980). It is noted here that in some cases of the short period fluctuations, the wave-like structure can hardly be seen and the sodium density enhances simultaneously at almost all altitudes of the layer as shown in Fig. 21.

The morphological study of the nighttime sodium layer observed with the lidar technique in northern Japan (38°N) are presented in this paper. The structural variations of the sodium layer with various time-scales suggest that the stratification of the sodium layer is related not only to the change in the composition of the atmosphere in the height range concerned, but also, to a large extent, to atmospheric tides or wave propagations.

Acknowledgments: Our sincere thanks are due to Dr. M. Jumonji of Hachinohe Institute of Technology for his effectual co-operation in developing the high-power dye laser for our lider system, and also to Messrs. T. Ohnuma, S. Okano, and K. Ide for their co-operation in carrying out observations.

References

Aruga, T., 1972: Study of the upper atmospheric sodium layer by a laser radar based on resonant scattering, *Ph.D. thesis, Tôhoku Univ., Japan.*

Aruga, T., H. Kamiyama, M. Jumonji, T. Kobayashi, and H. Inaba, 1974: Laser radar observation of the sodium layer in the upper atmosphere. *Rep. Ionos. Space Res. Japan.* **28**, 65-68.

Blamont, J.E., M.L. Chanin, and G. Megie, 1972: Vertical distribution and temperature profile of the night time atmospheric sodium layer obtained by laser backscatter, *Ann. Geophys.*, **28**, 833-838.

Clemsha, B.R., D.M. Simonich, P.P. Batista, and V.W.J.H. Kirchhoff, 1982: The diurnal variation of atmospheric sodium, *J. Geophys. Res.*, **87**, 181-186.

Gibson, A.J. and M.C.W. Sandford, 1971: The seasonal variation of the night-time sodium layer, *J. Atmos. Terr. Phys.*, **33**, 1675-1684.

Gibson, A.J. and M.C.W. Sandford, 1972: Daytime laser radar measurements of the atmospheric sodium layer, *Nature*, **239**, 509-511.

Handbook of Geophysics and Space Environments, 1965, Air Force Cambridge Res. Laboratories.

Hunten, D.M., 1967: Spectroscopic studies of the twilight airglow, *Space Sci. Rev.*, **6**, 493-573.

Kamiyama, H., F. Tomita, T. Ohnuma, S. Okano, and M. Jumonji, 1981: Flashlamp-pumped tunable laser radar system for the atmospheric sodium layer observation, *Tôhoku Geophys. Journ.*, **28**, 105-117.

Kirchhoff, V.W.J.H. and B.R. Clemsha, 1973: Atmospheric sodium layer measurements at 23°S, *J. Atmos. Terr. Phys.*, **35**, 1493-1498.

Megie, G. and J.E.Blamont, 1977: Laser sounding of atmospheric sodium interpretation in terms of global atmospheric parameters, *Planet. Space Sci.*, **25**, 1093-1109.

Megie, G., F. Bos, J.E.Blamont, and M.L.Chanin, 1978: Simultaneous nighttime lidar measurements of atmospheric sodium and potassium, *Planet. Space Sci.*, **26**, 27-35.

Richter, E.S., J.R. Rowlett, C.S. Gardner, and C.F. Sechrist, Jr., 1981: Lidar observation of the mesospheric sodium layer over Urbana, Illinois, *J. Atmos. Terr. Phys.*, **43**, 327-337.

Rowlett, J.R., C.S.Gardner, E.S. Richter, and C.F. Sechrist, Jr. 1978: Lidar observations of wave-like structure in the atmospheric sodium layer, *Geophys. Res. Lett.*, **5**, 683-686.

Shelton, J.D., C.S. Gardner, and C.F. Sechrist, Jr., 1980: Density response of the mesospheric sodium layer to gravity wave perturbations, *Geophys. Res. Lett.*, **7**, 1069-1072.

Simonich, D.M., B.R. Clemsha, and V.W.J.H. Kirchhoff, 1979: The mesospheric sodium layer at 23°S: nocturnal and seasonal variations, *J. Geophys. Res.*, **84**, 1543-1550.
U.S. Standard Atmosphere Supplements, 1966.